Particle Accelerators, 1987, Vol. 21, pp. 227–257
Photocopying permitted by license only

Printed in the United States of America

ANALYSIS OF THE ACCELERATION PROCESS IN A REBATRON†

D. DIALETIS,‡ S. J. MARSH,§ and C. A. KAPETANAKOS
Plasma Physics Division, Naval Research Laboratory, Washington, DC 20375

(Received January 2, 1986; in final form June 10, 1986)

A detailed numerical and analytical study of the beam dynamics in a rebatron accelerator has shown that energies approaching 1 GeV can be achieved within 5–10 μs. Since the acceleration in the rebatron occurs within a short time, the device may not be sensitive to the various instabilities, and the loss to synchrotron radiation should be small. The rapid acceleration is produced by convoluted parallel transmission lines, which provide a high-gradient electric field. At the initial stage of the acceleration, the beam is confined inside the torus by a strong focusing torsatron magnetic field, which makes the beam insensitive to the energy mismatch and to the external field index of a vertical magnetic field. This local field is generated by two coaxial cylindrical plates, located symmetrically around the major axis of the torus and carrying currents in opposite directions. The energy of the beam increases in synchronism with the vertical magnetic field so that the beam remains matched (i.e., the beam radius remains constant) during the entire acceleration. It was found that, as a result of the periodic nature of the acceleration, resonances can be excited, which cause the orbits to expand. The only disruptive resonance occurs at $\gamma \cong 1830$, i.e., when the vertical magnetic field reaches twice the value of the toroidal magnetic field.

1. INTRODUCTION

The electric field responsible for the acceleration of charged particles can be written as the sum of an electrostatic and an inductive component. The electrostatic component is generated by electric charges, and its divergence is proportional to the charge density, while its curl is zero. The inductive electric field, on the other hand, is generated by a time-varying magnetic field, and its curl is proportional to the rate of change of magnetic field, while its divergence is zero. It is the inductive field that is responsible for the acceleration in induction accelerators.[1–5]

Only modest acceleration can be achieved with electrostatic fields, because the maximum potential is limited by insulator flash-over. However, this is not the case with inductive fields, since the voltage is induced only in the circuit threading the flux, and the voltages of a sequence of circuits successively add to the energy W of the accelerated particle. The striking difference between the two fields becomes apparent when the orbit of the particle is circular. After a complete revolution, $W_2 - W_1 = 0$ for an electrostatic field, but $W_2 - W_1 \neq 0$ for an inductive

† This work was supported jointly by the Office of Naval Research and the U.S. Ballistic Research Laboratory, Aberdeen, MD.

‡ Permanent address: Science Applications, Inc., McLean, VA 22102.
§ Permanent address: Sachs/Freeman Associates, Bowia, MD 20715.

field, if the magnetic flux through the particle orbit changes with time. An additional advantage of induction accelerators is their inherently low impedance. As a result, these devices are ideally suited to drive high-current beams.

Quite naturally, induction accelerators are divided into linear and cyclic devices. The linear devices are in turn divided into three types: Astron-type,[6–9] Radlac-type,[10,11] and auto-accelerators.[12,13] In the first type, ferromagnetic induction cores are used to generate the accelerating field, while "air core" cavities are used in the second. In the auto-accelerator, the air core cavities are excited by the beam's self-fields rather than by external fields. Similarly, cyclic accelerators can be divided into two categories. In the first category belong those cyclic accelerators that use weak focusing to confine the electron beam, as in the conventional[14,15] and modified[14–18] betatrons. In the second category, beam confinement is achieved with strong focusing fields. This latter category includes the Stellatron,[19] racetrack,[20] and rebatron accelerators.[21] All three devices are currently in a rather preliminary state of development. In the last two devices,[20,21] the particle acceleration occurs rapidly, i.e., in a few microseconds, and thus limitations imposed by instabilities, field errors, and synchrotron radiation losses are substantially relaxed.

A rebatron[21] is shown schematically in Fig. 1. The high-gradient localized field responsible for the rapid acceleration is produced by two convoluted parallel transmission lines that feed the gap symmetrically, as in the Radlac II accelerator.[22] In an actual system, other transmission lines may be more

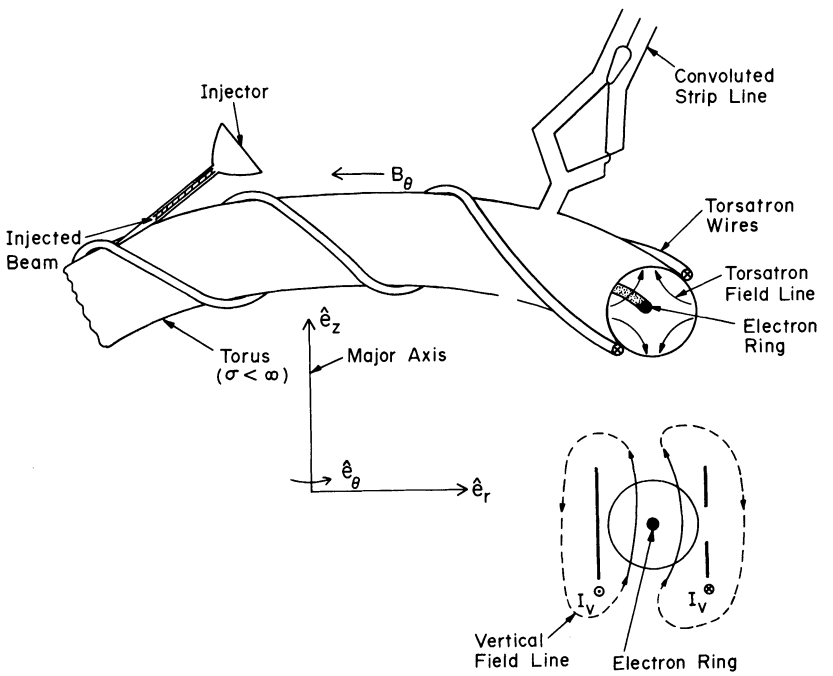

FIGURE 1 Schematic diagram of the rebatron. The two coaxial cylindrical plates are located symmetrically around the minor axis of the torus.

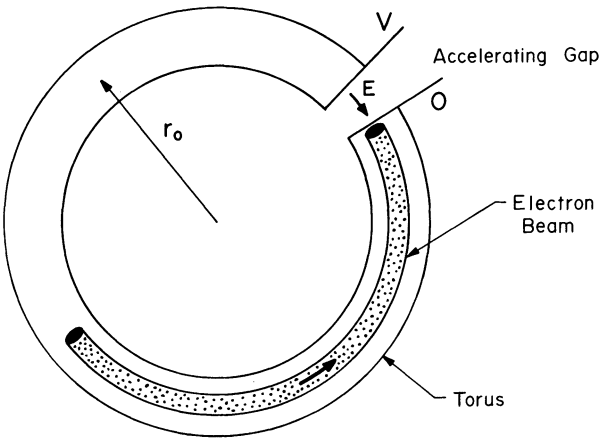

FIGURE 2 Top view of the rebatron, showing the beam and the accelerating gap.

appropriate. Since the acceleration occurs over a few microseconds, the constraints imposed on the vertical field are very stringent. To reduce the inductance of the coils, the vertical field is generated by two coaxial, cylindrical plates, as shown in the lower right corner of Fig. 1. The axes of these plates coincide with the major axis of the toroidal vessel and are located symmetrically around the minor axis of the torus. The purpose of the gap in the outer plate is to provide a field with the desirable external field index. The plates change mainly the local, vertical magnetic field, while the magnetic flux through the beam orbit remains approximately constant.

In the absence of losses, the output voltage of an open-ended transmission line that is suddenly shorted at the other end is a train of square pulses of alternating amplitude $+V$ to $-V$, where $+V$ is the charging voltage. If τ is the single-transit time of the electromagnetic wave in the line, the duration of the first pulse is τ, while the remaining pulses are of length 2τ. Only the longer pulses of the same polarity are used to accelerate the circulating beam. The duration of the longer pulses, i.e., 2τ, is selected to be equal to half the beam period around the major axis. The beam occupies only one half of the chamber and is synchronized to traverse the accelerating gap only when the correct-polarity (accelerating) pulse is present (Fig. 2). For a device with a $1-m$ major radius, the period of revolution around the major axis is approximately 20 ns; the transit time τ should therefore be about 5 ns.

To avoid shorting the gap, the L/R of the torus should be selected to be considerably longer than the applied pulse duration. Since, for a torus with a $1-m$ major radius and a 15-cm minor radius, $L \cong 2.5\,\mu$H, a surface resistivity around 1Ω/square will result in a $L/R \gg 2\tau$.

To achieve very high energies, a large number of pulses must be supplied by the transmission line. This implies that the energy losses of the line must be replenished in a time which will be typically less than 100 ns.

The mismatch between the beam energy and the vertical field is alleviated by a

strong focusing field. This field is generated by a set of $\ell = 2$ torsatron windings, i.e., two twisted wires that carry current in the same direction. In addition to the transverse components of the field, the torsatron windings provide a zero-order toroidal magnetic field. The beneficial effect of twisted quadrupole fields on the beam orbits has been recognized for several years.[23] In recent years, the $\ell = 2$ stellarator field has been used by Roberson *et al.* to improve the bandwidth of the modified betatron in a device named Stellatron[19] and also in the racetrack accelerator,[20] a device similar to the rebatron.

In recent studies,[21] we have demonstrated that the energy bandwidth of a rebatron accelerator can be very wide. In addition, we have shown that the torsatron windings substantially improve the current-carrying capabilities of the device and could alleviate the beam displacement problem associated with the diffusion of the self-magnetic-field. Therefore, it is expected that the limiting current in a rebatron would be determined from collective instabilities and not from the macroscopic stability of the beam orbits.

Beam capture in the rebatron, as in other devices that use strong focusing fields, is very difficult. The reason is that the strong focusing fields make the particle orbits insensitive to the energy mismatch, and thus, small changes in the vertical magnetic field are not sufficient to move the beam from the injection position near the wall to the minor axis of the torus. Recently, we have developed two injection schemes that appear very promising. One is based on the drag force of a resistive chamber wall[24] and the other on the modification of the beam orbit by a time-varying field.[25]

During acceleration, when the vertical magnetic field B_v far exceeds the torsatron field B_t, the beam dynamics is solely determined by the vertical and toroidal fields. For most applications of interest, $B_v \gg B_t$ at the peak of acceleration, and thus, beam extraction from the rebatron is similar to that from a modified betatron.[21]

In this report, we present results from our studies of the beam acceleration in a rebatron accelerator when the magnetic field varies with time. In Section 2, the applied electric and magnetic fields are described, and in Section 3, a simple theoretical model is examined and some important conclusions are derived from this model. The numerical results for an accelerated beam and their interpretation are given in Section 4. Finally, the conclusions of this investigation are presented in Section 5.

2. APPLIED FIELDS

2.1. Torsatron and External Toroidal Magnetic Fields

The magnetic field components of the $\ell = 2$ torsatron and external toroidal coils have been presented elsewhere[21] and will not be given here.

Notice that there is an additional constant $B_z^{(1)}$ component of the torsatron

magnetic field, given by

$$B_z^{(1)} = -\frac{1}{2\alpha r_0} B_0 \left(\ln \frac{8r_0}{\rho_0} - \frac{1}{2} \right). \tag{1}$$

This component arises from the fact that the currents in the two torsatron windings are in the same direction. (In a stellarator, this component is zero.) It is assumed in the rest of this paper that this undesirable component is canceled by adding an external magnetic field.

In the theoretical model formulated in Section 3, the toroidal corrections are neglected as well as all the terms with $m \geq 2$. Also, use is made of the cylindrical components B_r, B_θ, B_z in the global coordinate system $\hat{e}_r$, $\hat{e}_\theta$, $\hat{e}_z$ shown in Fig. 3. Their relation to the magnetic components in the local coordinate system $\hat{e}_\rho$, $\hat{e}_\phi$, $\hat{e}_s$ is as follows:

$$B_r = B_\rho \cos \phi - B_\phi \sin \phi, \tag{2a}$$

$$B_z = B_\rho \sin \phi + B_\phi \cos \phi, \tag{2b}$$

$$B_\theta = -B_s. \tag{2c}$$

Under these conditions, the magnetic field from the torsatron and the toroidal coils is approximately equal to

$$B_r \cong B_0 \varepsilon_1 [I_1(\bar{\rho}) \sin (\phi - 2\alpha s) + I_3(\bar{\rho}) \sin (3\phi - 2\alpha s)], \tag{3a}$$

$$B_z \cong B_0 \varepsilon_1 [I_1(\bar{\rho}) \cos (\phi - 2\alpha s) - I_3(\bar{\rho}) \cos (3\phi - 2\alpha s)], \tag{3b}$$

$$B_\theta \cong B_{\theta 0} + 2B_0 \varepsilon_1 I_2(\bar{\rho}) \cos (2\phi - 2\alpha s), \tag{3c}$$

where

$$\varepsilon_1 = \bar{\rho}_0 K_2'(\bar{\rho}_0), \tag{4a}$$

$$B_{\theta 0} = -B_{s0}^{\text{ext}} - B_0. \tag{4b}$$

In the numerical integration of the equations of motion for the centroid, the parameters in Table I were used.

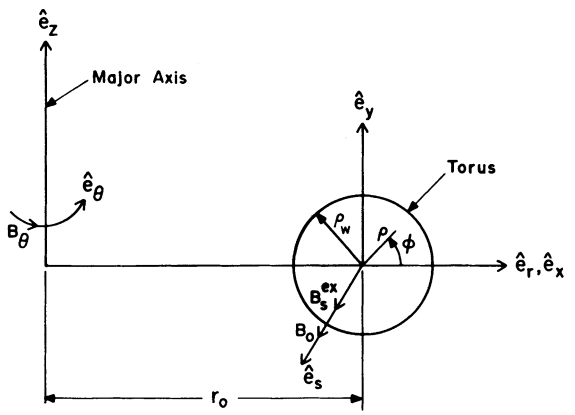

FIGURE 3 Systems of coordinates.

TABLE I

Parameters Associated with the Torsatron Fields Used in the Computer Runs

Torus major radius, r_0 (cm)	100
Toroidal chamber minor radius, ρ_w (cm)	10
Windings minor radius, ρ_0 (cm)	12
$\alpha = 2\pi/L$ (cm^{-1})	0.1
$\varepsilon_1 = 2\alpha\rho_0 K_2'(2\alpha\rho_0)$	−0.481
ℓ	2
Winding current, I_0 (kA)	140
Torsatron magnetic field, B_0 (kG)	5.6
External toroidal field B_{s0}^{ext} (kG)	10

2.2. *Vector Potential and Magnetic Field of the Plates*

Let a single cylindrical plate of width b and height h, where $b \ll h$, be located so that the axis of the cylinder coincides with the major axis of the torus and the distance of the plate from the minor axis of the torus is equal to a. For a homogeneous current density with a single component $J_\theta = I_p/bh$, where I_p is the current flowing in the plate, the vector potential A_θ is

$$A_\theta = \frac{I_p}{c}\hat{A}_\theta, \tag{5}$$

where

$$\hat{A}_\theta(x, z, r_0, a, h, b) = \frac{4}{bh}\int_{a-(b/2)}^{a+(b/2)} dx' \int_{-h/2}^{h/2} dz' \frac{\left(\dfrac{r_0 + x'}{r_0 + x}\right)^{1/2}}{\sqrt{1 - k'^2}} \left[\tfrac{1}{2}(1 + k'^2)K'(k') - E'(k')\right] \tag{6a}$$

and

$$k'^2 = \frac{(x - x')^2 + (z - z')^2}{(2r_0 + x + x')^2 + (z - z')^2}. \tag{6b}$$

The point (x, z), where $\hat{A}_\theta$ is computed, is in the local coordinate system $\hat{e}_x$, $\hat{e}_z$, $\hat{e}_s$ of Fig. 3, and $K'(k')$, $E'(k')$ are the complete elliptic integrals. When the plate is located close to the torus, so that $a/r_0 \ll 1$, and one is interested in the vector potential only inside the torus, then $k'^2 \ll 1$ and the elliptic integrals can be expanded[26] with respect to k'^2. To lowest order, $\hat{A}_\theta$ is given by

$$\begin{aligned}\hat{A}_\theta(x, z, r_0, a, h, b) &\cong -\frac{2}{bh}\int_{a-(b/2)}^{a+(b/2)} dx' \int_{-h/2}^{h/2} dz' \left(\frac{r_0 + x'}{r_0 + x}\right)^{1/2} \left(\tfrac{1}{2}\ln\frac{k'^2}{16} + 2\right) \\ &\cong -\frac{2}{bh}\int_{a-(b/2)}^{a+(b/2)} dx' \int_{-h/2}^{h/2} dz' \left\{-\frac{1}{2}\frac{x' + x}{r_0} + \left(1 + \frac{1}{2}\frac{x' - x}{r_0}\right)\right. \\ &\quad \left. \times \left[\tfrac{1}{2}\ln\frac{(x' - x)^2 + (z' - z)^2}{(8r_0)^2} + 2\right]\right\},\end{aligned} \tag{7}$$

which contains the toroidal corrections to the lowest order in a/r_0. A further simplification arises from the fact that $b \ll h$, so that $\hat{A}_\theta$ is computed in the limit $b \to 0$. Then the integrals in Eq. (7) can be computed exactly and $\hat{A}_\theta$ is equal to

$$\hat{A}_\theta(x, z, r_0, a, h, 0) \cong \frac{a+x}{r_0} - 2\left(1+\frac{1}{2}\frac{a-x}{r_0}\right)\left[1+\frac{a-x}{h}\left(\arctan\frac{\frac{h}{2}+z}{a-x}+\arctan\frac{\frac{h}{2}-z}{a-x}\right)+\frac{1}{2}\frac{\frac{h}{2}+z}{h}\ln\frac{\left(\frac{h}{2}+z\right)^2+(a-x)^2}{(8r_0)^2}+\frac{1}{2}\frac{\frac{h}{2}-z}{h}\ln\frac{\left(\frac{h}{2}-z\right)^2+(a-x)^2}{(8r_0)^2}\right]. \quad (8)$$

The B_r, B_z components of the magnetic field near the plate (and therefore inside the torus), to lowest order in a/r_0, are equal to

$$B_r = \frac{I_p}{c}\hat{B}_r, \quad (9a)$$

$$B_z = \frac{I_p}{c}\hat{B}_z, \quad (9b)$$

where

$$\hat{B}_r = -\frac{\partial \hat{A}_\theta}{\partial z}, \quad (10a)$$

$$\hat{B}_z = \frac{\partial \hat{A}_\theta}{\partial x}+\frac{1}{r_0}\hat{A}_\theta. \quad (10b)$$

Substitution of Eq. (8) into Eqs. (10a) and (10b) leads to the expressions

$$\hat{B}_r = \frac{1}{h}\left(1+\frac{1}{2}\frac{a-x}{r_0}\right)\ln\frac{\left(\frac{h}{2}+z\right)^2+(a-x)^2}{\left(\frac{h}{2}-z\right)^2+(a-x)^2}, \quad (11a)$$

and

$$\hat{B}_z = \frac{2}{h}\left(\arctan\frac{\frac{h}{2}+z}{a-x}+\arctan\frac{\frac{h}{2}-z}{a-x}\right) - \frac{1}{2r_0}\left[\frac{\frac{h}{2}+z}{h}\ln\frac{\left(\frac{h}{2}+z\right)^2+(a-x)^2}{(8r_0)^2}+\frac{\frac{h}{2}-z}{h}\ln\frac{\left(\frac{h}{2}-z\right)^2+(a-x)^2}{(8r_0)^2}\right]. \quad (11b)$$

In the limit $r_0 \to \infty$, Eqs. (10) and (11) reduce the magnetic field of an infinite-length slab, as they should.

The particle orbits are not stable unless the external field index n of the vertical magnetic field is in the region $0 < n < 1$. Such a field can be generated by a set of two plates which surround the torus (see Fig. 1), with the outer plate having a gap symmetrically located in the middle of the plate. From the vector potential for a single plate, it is easy to compute the vector potential of the outer plate with a gap of height H_0. This vector potential is given by

$$\hat{A}_{\theta+} = \frac{h}{h - H_0}\hat{A}_\theta(x, z, r_0, a, h, 0) - \frac{H_0}{h - H_0}\hat{A}_0(x, z, r_0, a, H_0, 0). \tag{12a}$$

The current density in the presence of a gap is proportional to $I_p/(h - H_0)$. The first term in Eq. (12a) is the contribution to $\hat{A}_{\theta+}$ from the whole plate (of height h), and the second term is the contribution of the gap (of height H_0), which should be subtracted. Since the inner plate is located at a distance $-a$ from the minor axis and carries a current $-I_p$, its vector potential is

$$\hat{A}_{\theta-} = -\hat{A}_\theta(x, z, r_0, -a, h, 0). \tag{12b}$$

and the combined potential from both plates is

$$A_\theta = \frac{I_p}{c}(\hat{A}_{\theta+} + \hat{A}_{\theta-}). \tag{13}$$

The magnetic field is computed with the help of Eqs. (9) through (13). Near the minor axis, the magnetic field simplifies to the following linearized expressions:

$$B_r = -B_{z0}n_0\frac{z}{r_0}, \tag{14a}$$

$$B_z = B_{z0}\left(1 - n_0\frac{x}{r_0}\right), \tag{14b}$$

where

$$\begin{aligned} n_0 &\equiv -\frac{r_0}{B_{z0}}\left(\frac{\partial B_z}{\partial x}\right)_{\substack{x=0\\z=0}} \\ &\equiv -\frac{r_0}{B_{z0}}\left(\frac{\partial B_r}{\partial z}\right)_{\substack{x=0\\z=0}} \\ &= \frac{\dfrac{r_0}{2a}\dfrac{H_0}{2a}\dfrac{h}{2a}\left(1 + \dfrac{1}{2}\dfrac{a}{r_0}\right)\left(1 + \dfrac{H_0}{h}\right) - \dfrac{1}{2}\dfrac{\dfrac{h}{2a}}{1 + \left(\dfrac{h}{2a}\right)^2}}{\arctan\dfrac{h}{2a}}, \end{aligned} \tag{15a}$$

$$B_{z0} = \frac{I_p}{c}\hat{B}_{z0}, \tag{15b}$$

$$\hat{B}_{z0} = \frac{8}{h}\arctan\frac{h}{2a} + \frac{H_0}{h - H_0}\left[\frac{4}{h}\arctan\frac{h}{2a} - \frac{4}{H_0}\arctan\frac{H_0}{2a} - \frac{1}{2r_0}\ln\frac{1 + \left(\dfrac{h}{2a}\right)^2}{1 + \left(\dfrac{H_0}{2a}\right)^2}\right]. \tag{15c}$$

Equations (14a) and (14b) are identical in form to the linearized betatron field in the modified betatron. According to Eq. (15a), the external field index n_0 at $x = z = 0$ is sensitive to the height H_0 of the gap. In particular, if there is no gap in the outer plate (i.e., $H_0 = 0$), then n_0 becomes negative.

The magnetic field components of the plates are plotted without a gap in Fig. 4 and with a gap in the outer plate in Fig. 5. The various parameters for these plots are listed in Table II. The effect of the gap in the magnetic field is quite prominent. In the absence of a gap, n_0 changes from positive to negative as r increases from 90 to 110 cm for z less than 10 cm. On the other hand, when the gap is present, n_0 has the desired value of 0.5 near the minor axis of the torus (i.e., in the linear regime), but as one approaches the gap, n_0 varies from positive to negative as z increases from zero to 10 cm. Figures 4b and 5b, and 4d and 5d show the variation of B_r versus r and B_z versus z, respectively, for various values

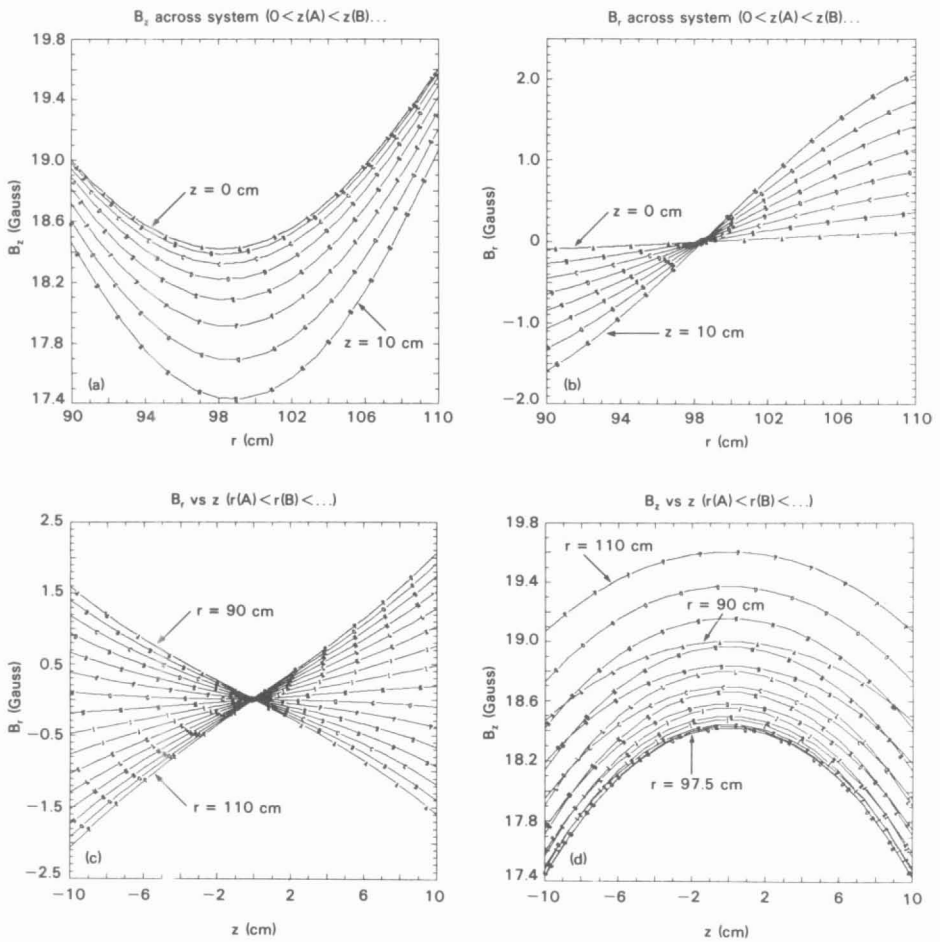

FIGURE 4 Magnetic field of plates without a gap in the outer plate, at various distances along the r or z axis. (a) B_z versus r, (b) B_r versus r, (c) B_r versus z, and (d) B_z versus z.

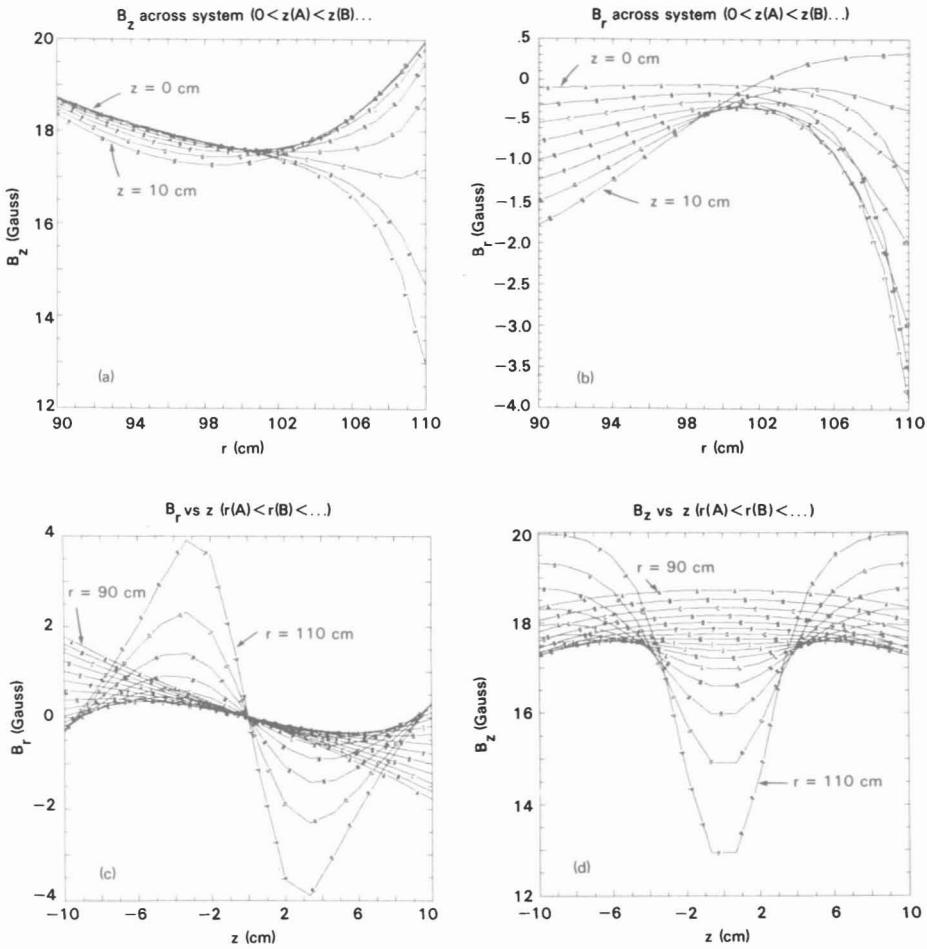

FIGURE 5 Magnetic field of plates with a gap in the outer plate, at various distances along the r or z axis. (a) B_z versus r, (b) B_r versus r, (c) B_r versus z, and (d) B_z versus z.

of z or r. Ideally, they should be straight lines, parallel to the horizontal axis, in the region of interest. As may be seen from Fig. 5, this is the case when there is a gap. Although only the first-order toroidal corrections were retained, they are quite noticeable. For example, in Fig. 4a at $z = 0$, there is a difference of 0.6 G/kA in the values of B_z at $r = 90$ cm and $r = 110$ cm, due to the toroidal correction. Finally, it should be pointed out that, because of the gap, the value of the vertical magnetic field at the minor axis drops from 18.45 G/kA to 17.58 G/kA.

As already mentioned, in order to keep the beam matched, the current in the plates should increase in synchronism with the energy of the beam. Therefore, there is an electric field E_p associated with the time-dependent vector potential of

TABLE II

Parameters Associated with the Magnetic Field of the Plates Shown in Figs. 4 and 5

	Fig. 4	Fig. 5
Torus major radius, r_0 (cm)	100	100
Toroidal chamber minor radius, ρ_w (cm)	10	10
Outer plate distance from minor axis, a_0 (cm)	12	12
Inner plate distance from minor axis, a_i (cm)	−12	−12
Half-height of outer plate, $h_0/2$ (cm)	24	24
Half-height of outer gap, $H_0/2$ (cm)	0	2.35
Half-height of inner plate, $h_i/2$ (cm)	24	24
Current in outer plate, I_p (kA)	1	1
B_z at minor axis (G)	18.45	17.58
External field index at minor axis, n_0	−0.18	0.5
Acceleration correction factor, η_p	1.038	1.035

the plates, namely,

$$E_p = -\frac{1}{c}\frac{\partial A_\theta}{\partial t} = -\frac{\dot{I}_p}{c^2}(\hat{A}_{\theta+} + \hat{A}_{\theta-}). \tag{16}$$

As shown in Section 3, this electric field will have an effect on the rate of change of the current in the plates.

2.3. *The Accelerating Electric Field*

The accelerating electric field in the gap has been given elsewhere.[21] In order to achieve a faster convergence of the series that expresses this field, the configuration shown in Fig. 6a was chosen. Also, the first-order toroidal corrections were included in the calculations. It was necessary to do so since, as will be shown in Section 3, the toroidal corrections of the accelerating electric field cancel the first-order contribution from the electric field of the plates [Eq. (16)] in the expression for the mismatch $\delta\gamma/\gamma$, and as a consequence, the drift of the particle orbits is, for all practical purposes, zero.

The electric field lines and field components are plotted in Figs. 6b, 6c, and 6d. The various parameters for these plots are listed in Table III. The dotted lines in Fig. 6b indicate the location of the accelerating gap. In Fig. 6c, the Gibbs phenomenon is quite noticeable at $\rho = \rho_w = 10$ cm, where the E_s component is discontinuous. As expected, the line integral along the s axis and at any radius ρ is equal to V_0. As may be seen from Fig. 6d, the E_ρ component changes sign as s increases, and therefore, on the average, it has little effect on the particle orbits. The poloidal component E_ϕ was not plotted, since it is zero at $\phi = 0$. In general, it is small and its contribution to the particle orbits is negligible.

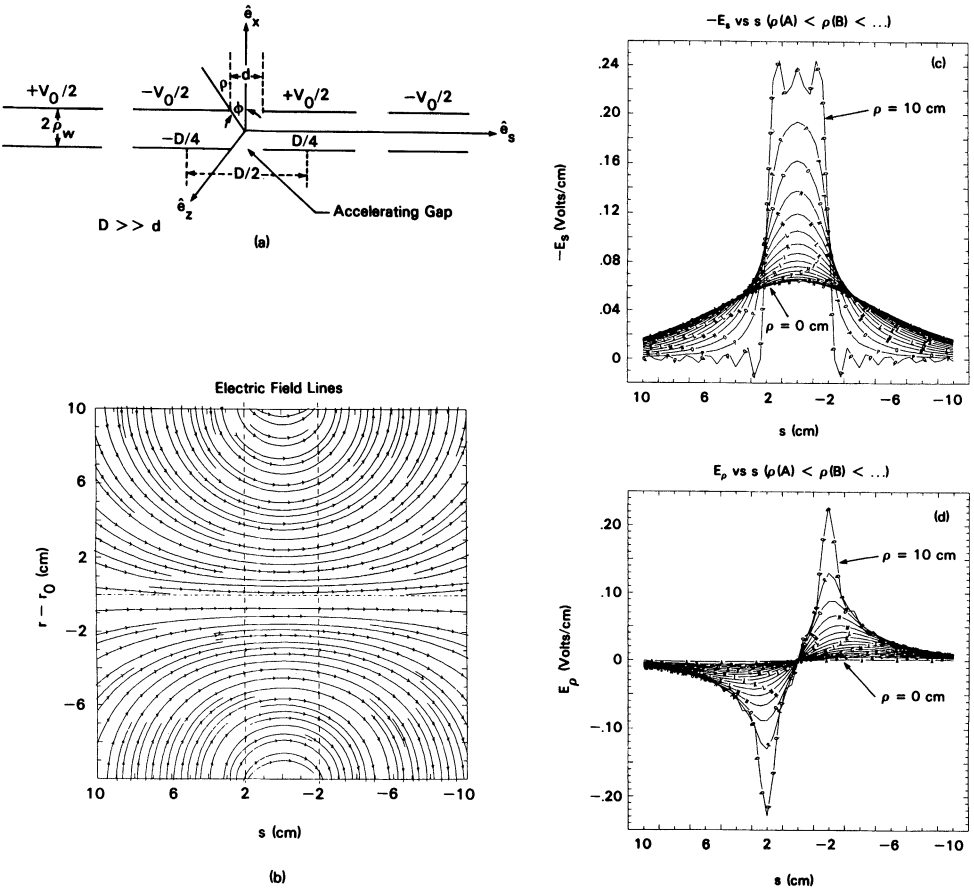

FIGURE 6 Configuration (a), field lines (b), and cylindrical components (c and d) of the accelerating electric field in the region of the gap at various distances from the minor axis. The toroidal corrections have been included.

TABLE III

Parameters Associated with the Accelerating Field in the Region of the Gap shown in Fig. 6

Torus major radius, r_0 (cm)	100
Toroidal chamber minor radius, ρ_w (cm)	10
Half-width of the gap, $d/2$ (cm)	2
Half-period of structure, $D/2$ (cm)	62
Voltage, V_0 (V)	1
Poloidal angle, ϕ (radians)	0

3. SIMPLE THEORETICAL MODEL

3.1. Approximate Equations of Motion and Conservation Law

The exact equations of motion are too complicated to provide any insight into the effect that the torsatron and vertical magnetic fields have on the particle orbits. A better understanding is gained by a simple model which provides fairly accurate results and is based on the assumption that the toroidal velocity v_θ of the particle, being very close to the velocity of light, remains constant (though of course the energy does not). In this case,

$$s = -v_\theta t, \tag{17}$$

and the remaining equations of the motion are

$$\frac{d}{dt}(\gamma\dot{r}) - \gamma r\dot{\theta}^2 = -\frac{e}{mc}(v_\theta B_z - \dot{z}B_\theta), \tag{18a}$$

$$\frac{d}{dt}(\gamma\dot{z}) = -\frac{e}{mc}(\dot{r}B_\theta - v_\theta B_r). \tag{18b}$$

For simplicity, the image fields will be neglected in the present analysis. Also, the magnetic field of the torsatron and toroidal coils is given by the simplified Eqs. (3) and that of the plates by Eqs. (14). In Eqs. (3), $2\alpha s$ is replaced by $-\omega_w t$ [see Eq. (17)], where

$$\omega_w = 2\alpha v_\theta. \tag{19}$$

We now set $x = r - r_0$ and define the complex amplitude

$$u = x + iz = \rho e^{i\phi}. \tag{20}$$

Then Eqs. (18a) and (18b) can be combined into one complex equation of motion, namely,

$$\begin{aligned}\ddot{u} + i\left[\frac{\Omega_{\theta 0}}{\gamma} + 2\varepsilon_1\frac{\Omega_0}{\gamma}I_2(\tilde{\rho})\cos(2\phi + \omega_w t) - i\frac{\dot{\gamma}}{\gamma}\right]\dot{u} \\ + \varepsilon_1\omega_w\frac{\Omega_0}{\gamma}[I_1(\tilde{\rho})e^{-i(\phi+\omega_w t)} - I_3(\tilde{\rho})e^{i(3\phi+\omega_w t)}] \\ + \omega_\perp^2 u + \delta\omega^2 u^* = v_\theta\left(\frac{v_\theta}{r_0} - \frac{\Omega_{z0}}{\gamma}\right),\end{aligned} \tag{21}$$

where

$$\omega_\perp^2 = \tfrac{1}{2}\omega_0^2, \tag{22a}$$

$$\delta\omega^2 = \tfrac{1}{2}\omega_0^2 - n_0\frac{v_\theta}{r_0}\frac{\Omega_{z0}}{\gamma}, \tag{22b}$$

$$\omega_0 = \frac{v_\theta}{r_0}, \tag{22c}$$

and $\Omega_{\theta 0}$, Ω_0, Ω_{z0} are the nonrelativistic cyclotron frequencies associated with the magnetic fields $B_{\theta 0}$, B_0, B_{z0} [i.e., $\Omega = (e/mc)B$]. The quantity $2\pi/\omega_0$ is the time it takes a particle on the minor axis to make one revolution around the torus. Moreover, the rate of change of γ is mainly due to the s components of the electric fields of the transmission line and the plates, so that

$$\dot{\gamma} \cong -\frac{e}{mc^2} v_\theta (E_{\text{gap}} + E_p), \tag{23}$$

where E_{gap} is the accelerating electric field and E_p is given by Eq. (16).

Equation (21) is still too difficult to handle. But it leads to a conservation law when the fast motion which oscillates with frequency ω_w is averaged out. Details may be found elsewhere.[24] Here we give only the final result, which was obtained with the assumptions that γ remains constant and that $\omega_w \ll |\Omega_{\theta 0}|/\gamma$. Under these conditions, the conservation law becomes

$$(1-n_0)\left(\frac{X}{r_0} - \frac{\delta\gamma/\gamma}{1-n_0}\right)^2 + n_0\left(\frac{Z}{r_0}\right)^2 + \left(\frac{2\omega_0}{\omega_w}\right)^2 [b_- I_1^2(2\alpha R) + b_+ I_3^2(2\alpha R)] = K, \tag{24}$$

where

$$\frac{\delta\gamma}{\gamma} = \frac{\gamma - \gamma_0}{\gamma}, \tag{25a}$$

$$\gamma_0 = \frac{\Omega_{z0} r_0}{v_\theta}, \tag{25b}$$

$$b_\pm = \frac{\left(\frac{1}{2}\varepsilon_1 \dfrac{B_0}{B_{z0}}\right)^2}{1 \pm \dfrac{\omega_0}{\omega_w}\dfrac{B_{\theta 0}}{B_{z0}}}. \tag{25c}$$

Here K is the constant of integration and is determined from the initial conditions, (X, Z) is the average (or guiding-center) position of the beam centroid, $R = (X^2 + Z^2)^{1/2}$, γ_0 is the value of γ that matches the vertical magnetic field B_z from the plates when the beam centroid is at $X = Z = 0$ (i.e., at the origin of the local coordinate system), and $\delta\gamma/\gamma$ is the mismatch between the actual value of γ and γ_0. When the mismatch is equal to zero, then the beam is matched at the origin, i.e., the point $X = Z = 0$ is an equilibrium position.

Consider the special case when $2\alpha R \ll 1$ and $\delta\gamma/\gamma \ll 1$. Then Eq. (24), which is actually an equation for the particle orbits, simplifies to the following expression:

$$(b_- + 1 - n_0)\left(\frac{X}{r_0} - \frac{\delta\gamma/\gamma}{b_- + 1 - n_0}\right)^2 + (b_- + n_0)\left(\frac{Z}{r_0}\right)^2 = K'. \tag{26}$$

where K' is a new integration constant. This equation describes either an ellipse or a hyperbola centered at $(\Delta r, 0)$, where

$$\frac{\Delta r}{r_0} = \frac{\delta\gamma/\gamma}{b_- + 1 - n_0}. \tag{27}$$

At the initial stage of the acceleration, the torsatron magnetic field B_0 is much larger than the vertical magnetic field B_{z0}, i.e., $|B_0/B_{z0}| \gg 1$. Since the external field index n_0 is of order one, it follows that $|b_-|$ is much greater than unity, or $|n_0|$ or $|1-n_0|$, and Eq. [26] simplifies to the relation

$$\left(\frac{X}{r_0} - \frac{\delta\gamma/\gamma}{b_-}\right)^2 + \left(\frac{Z}{r_0}\right)^2 = K'. \tag{28}$$

It is seen then that in the presence of the torsatron field, at the initial stage of the acceleration, the orbits on the (r, z) plane are circles centered at

$$\frac{\Delta r}{r_0} \cong \frac{\delta\gamma/\gamma}{b_-}. \tag{29}$$

This orbit displacement is independent of the external field index n_0, and since $|b_-| \gg 1$, it is not sensitive to the value of the mismatch $\delta\gamma/\gamma$—i.e., the torsatron field, which dominates at the initial stage of the acceleration, confines the beam inside the torus.

At a later stage of the acceleration, as the vertical magnetic field increases synchronously with the energy of the beam, it becomes eventually greater than B_0, and the condition $|b_-| \ll 1$ holds. In this case, Eq. (26) reduces to the expression

$$(1-n_0)\left(\frac{X}{r_0} - \frac{\delta\gamma/\gamma}{1-n_0}\right)^2 + n_0\left(\frac{Z}{r_0}\right)^2 = K'. \tag{30}$$

Therefore, in order to have closed orbits during the whole duration of the acceleration, the condition $0 < n_0 < 1$ must be satisfied, and it is this condition that requires the presence of a gap on the outer plate, as indicated in Section 2. Also, in this case,

$$\frac{\Delta r}{r_0} \cong \frac{\delta\gamma/\gamma}{1-n_0}, \tag{31}$$

which is sensitive to the mismatch $\delta\gamma/\gamma$ and to the external field index n_0. In the special case where $n_0 = 0$, the orbits are given by the relation $X =$ constant, i.e., they describe a vertical motion, and this may provide a possible means of extracting the beam from the toroidal chamber.

3.2. Rate of Change of the Current in the Plates

As mentioned in the previous sections, the two coaxial cylindrical plates generate a local vertical magnetic field which increases synchronously with the beam energy so that the major radius of the ring remains approximately constant. From Eq. (23), a particle at the origin of the local coordinate system $\hat{e}_\rho$, $\hat{e}_\phi$, $\hat{e}_s$ will gain energy at the rate given by

$$\dot{\gamma} \cong -\frac{e}{mc}\left(\frac{V_0}{2\pi r_0} - \frac{\dot{I}_p}{c^2}\hat{A}_{\theta 0}\right). \tag{32}$$

Equation (32) has been derived from Eqs. (5) and (16) and by taking the average accelerating field in the gap as equal to $E_{\text{gap}} = V_0/2\pi r_0$. The quantity $\hat{A}_{\theta 0}$ is given by

$$\hat{A}_{\theta 0} = \frac{a}{r_0}\left[\ln\frac{\left(\frac{8r_0}{a}\right)^2}{1+\left(\frac{h}{2a}\right)^2} - \frac{4a}{h}\arctan\frac{h}{2a}\right] - 2\frac{H_0}{h-H_0}\left(1+\frac{1}{2}\frac{a}{r_0}\right)$$

$$\times\left[\frac{2a}{h}\arctan\frac{h}{2a} - \frac{2a}{H_0}\arctan\frac{H_0}{2a} + \tfrac{1}{2}\ln\frac{1+\left(\frac{h}{2a}\right)^2}{1+\left(\frac{H_0}{2a}\right)^2}\right]. \tag{33}$$

The beam will remain matched at the origin during the acceleration when [see Eqs. (25b), (15b), and (15c)]

$$\dot{\gamma} = \frac{\dot{I}_p}{c^2}\frac{e}{mc}\hat{B}_{z0}r_0. \tag{34}$$

From Eqs. (32) and (34), it follows that the rate of change of the current in the plates should be equal to

$$\frac{1}{c^2}\dot{I}_p = -\frac{V_0}{2\pi r_0^2}\frac{\eta_p}{\hat{B}_{z0}}, \tag{35a}$$

where

$$\eta_p = \frac{1}{1-\frac{1}{r_0}\frac{\hat{A}_{\theta 0}}{\hat{B}_{z0}}}. \tag{35b}$$

The parameter η_p is the acceleration correction factor due to the electric field on the plates and has been listed in Table II.

It is interesting to show that even when the beam centroid is slightly off the origin at some later time, the mismatch $\delta\gamma$ is still zero to first order in the displacement from the origin if $\delta\gamma$ was initially zero. If the beam is at some position $r = r_0 + x$, the average accelerating field is equal to $E_{\text{gap}} = V_0/2\pi r$ and the vector potential at that position is proportional to $\hat{A}_{\theta 0} + (\partial\hat{A}_0/\partial x)\,x$, where the partial derivative is evaluated at the origin. Therefore, from Eqs. (25a), (25b), and (23), it follows that

$$\frac{d\delta\gamma}{dt} = -\frac{e}{mc}\left[\frac{V_0}{2\pi(r_0+x)} - \frac{\dot{I}_p}{c^2}\left(\hat{A}_{\theta 0} + \frac{\partial\hat{A}_\theta}{\partial x}x\right) + \frac{\dot{I}_p}{c^2}\hat{B}_{z0}r_0\right]$$

$$\cong -\frac{e}{mc}\left[\frac{V_0}{2\pi r_0} + \frac{\dot{I}_p}{c^2}r_0\left(\hat{B}_{z0} - \frac{1}{r_0}\hat{A}_{\theta 0}\right) - \left(\frac{V_0}{2\pi r_0^2} + \frac{\dot{I}_p}{c^2}\frac{\partial\hat{A}_\theta}{\partial x}\right)x\right] = 0. \tag{36}$$

In deriving Eq. (36), we used Eqs. (35a) and (10b). It is seen then that, in the rate of change of $\delta\gamma$ associated with the slow motion of the beam, the first-order

effect of the plates is canceled by the first-order toroidal corrections of the accelerating field. Therefore, the toroidal corrections (especially the $1/r$ dependence) of the accelerating field must be incorporated in the equations of motion. Otherwise, there is a slow drift of the beam in the radial direction. This has been observed in several computer runs which have not included the toroidal corrections. After the toroidal corrections were included, the drift of the particle orbits became negligible.

3.3. Resonances with Multiple Frequencies in the Rebatron

In contrast to the modified betatron, where the acceleration takes place continuously, it is a stepwise process in the rebatron, since the accelerating field is localized at the gap. Therefore, there is a periodicity associated with the rise of the beam energy, with period $T = 2\pi/\omega_0$, i.e., equal to the time it takes the particle to make a full turn around the torus. Let the increment per turn in γ be $\Delta\gamma$. Since the increase of γ takes place during the short time Δt that the particle takes to cross the accelerating gap, and since $\Delta t \ll T$, γ is a ladder function with step $\Delta\gamma$ and length T. Therefore, γ can be expressed as follows:

$$\gamma(t) = \gamma_{\text{lin}}(t) + \gamma_{\text{osc}}(t), \tag{37a}$$

where

$$\gamma_{\text{lin}}(t) = \gamma_i + \Delta\gamma\left(\frac{1}{2} + \frac{t}{T}\right), \qquad 0 \le t < \infty, \tag{37b}$$

$$\gamma_{\text{osc}}(t) = \Delta\gamma\left(\frac{1}{2} - \frac{t}{T}\right), \qquad 0 \le t \le T, \tag{37c}$$

and $\gamma_{\text{osc}}(t + T) = \gamma_{\text{osc}}(t)$. Since the first crossing of the accelerating gap occurs at time $t = 0$, after m turns γ is equal to $\gamma = \gamma_i + (m + 1)\Delta\gamma$, where γ_i is the initial value of γ.

Since $\gamma_{\text{osc}}(t)$ is a periodic function, it can be Fourier analyzed, i.e.,

$$\gamma_{\text{osc}}(t) = \frac{\Delta\gamma}{\pi} \sum_{n=1}^{\infty} \frac{1}{n} \sin(n\omega_0 t). \tag{38}$$

As γ increases, the stage is reached where $|\Omega_{\theta 0}/\gamma| \ll \omega_w$, whereupon the torsatron field is no longer effective and can be dropped from the equations of motion. Then, Eq. (21) reduces to the relation

$$\ddot{u} + i\frac{\Omega_{\theta 0}}{\gamma}\dot{u} + \tfrac{1}{2}\omega_0^2 u = \frac{c^2}{\gamma r_0}\left(\gamma - \frac{\Omega_{z0} r_0}{c}\right), \tag{39}$$

where, for simplicity, we set $n_0 = 1/2$ and $v_\theta \cong c$. Since the vertical magnetic field B_{z0} matches at all times the linear part of γ [see Eq. (37b)], and since eventually $|\gamma_{\text{osc}}(t)| \ll \gamma_{\text{lin}}(t)$, Eq. (39) can be written approximately as

$$\ddot{u} + i\frac{\Omega_{\theta 0}}{\gamma_{\text{lin}}}\dot{u} + \tfrac{1}{2}\omega_0^2 u \cong \frac{c^2}{\gamma_{\text{lin}} r_0}\frac{\Delta\gamma}{\pi}\sum_{n=1}^{\infty}\frac{1}{n}\sin(n\omega_0 t). \tag{40}$$

This is a linear second-order differential equation with characteristic frequencies equal to

$$\omega_{\pm} = \tfrac{1}{2}(\sqrt{\varepsilon^2 + 2} \pm |\varepsilon|)\omega_0, \tag{41a}$$

$$|\varepsilon| = \frac{|\Omega_{\theta 0}|}{\gamma_{\text{lin}}\omega_0} = \frac{|B_{\theta 0}|}{B_{z0}}. \tag{41b}$$

Therefore a resonance is excited when $\omega_+ = n\omega_0$, $n = 1, 2, 3, \ldots$, or, in terms of $|\varepsilon|$, when

$$\frac{1}{|\varepsilon|} \equiv \frac{B_{z0}}{|B_{\theta 0}|} = \frac{2n}{2n^2 - 1}. \tag{42}$$

A similar expression has been obtained for a periodic disturbance in the modified betatron.[27] The difference here is that the occurrence of resonances in the rebatron is an inherent property of the device due to the localized accelerating electric field and the periodic nature of the acceleration. According to Eq. (25b), resonance occurs each time $\gamma \cong \gamma_n$, where

$$\gamma_n = \frac{2n}{2n^2 - 1} \frac{|\Omega_{\theta 0}|\, r_0}{c}, \tag{43}$$

and $n = 1, 2, \ldots$. As will be shown in Section 4, these resonances cause the orbits to expand, and, in the worst case (i.e., when $n = 1$), the beam hits the wall of the torus.

It is apparent from Eq. (41a) that $\omega_- < \omega_+$ always. But, as the vertical magnetic field increases, ω_+ may become a multiple of ω_-, i.e., $\omega_+ = m\omega_-$. In terms of $|\varepsilon|$, this happens when

$$\frac{1}{|\varepsilon|} = \frac{B_{z0}}{|B_{\theta 0}|} = \frac{\sqrt{2m}}{m - 1}, \tag{44}$$

where $m = 2, 3, \ldots$. The occurrence of a multiple frequency changes the orbits into triangular or square shapes, depending on the value of m. According to Eq. (25b), a multiple frequency occurs each time $\gamma \cong \gamma_m$, where

$$\gamma_m = \frac{\sqrt{2m}}{m - 1} \frac{|\Omega_{\theta 0}|\, r_0}{c}, \tag{45}$$

and $m = 2, 3, \ldots$. This has been observed in computer runs, and examples will be given in Section 4.

4. NUMERICAL RESULTS AND THEIR INTERPRETATION

The various properties of the rebatron were investigated by integrating the relativistic equations of motion for the beam centroid using Eqs. (9) through (13) for the magnetic field of the plates and Eq. (16) for the electric field of the plates. The various parameters and their values are listed in Tables I through III. The image fields of the beam were not included in the computations.

To test the extent over which the external field index effectively confines the particle orbits, some computer runs without acceleration at $\gamma = 387$ were made, assuming the presence of a gap in the outer plate. The vertical magnetic field was set equal to $B_{z0} = 6597$ G (i.e., it matches the value of $\gamma_0 = 387$). The results for various initial conditions are shown in Fig. 7. As expected, when the centroid is initially at the origin, it remains there, since γ and B_z are matched at that position. On the other hand, since the external field index depends on position and is close to unity at $X = 6$ cm, $z = 0$ (see Fig. 5a), when the particle is placed there initially, it moves in a outward radial direction [see Eq. (30)] and eventually strikes the wall. Therefore, for the parameters chosen, the particle is successfully confined inside the torus up to distances of 5 cm from the minor axis.

In order to test the focusing effect of the torsatron magnetic field at the initial stage of the acceleration, a set of runs was made without a gap in the outer plate so that $n_0 \cong -0.18$. The results are shown in Fig. 8. The initial vertical magnetic fields were $B_{z0} = 341$ G (it matches $\gamma_0 = 20$) in Fig. 8a, $B_{z0} = 3.41$ kG (it matches

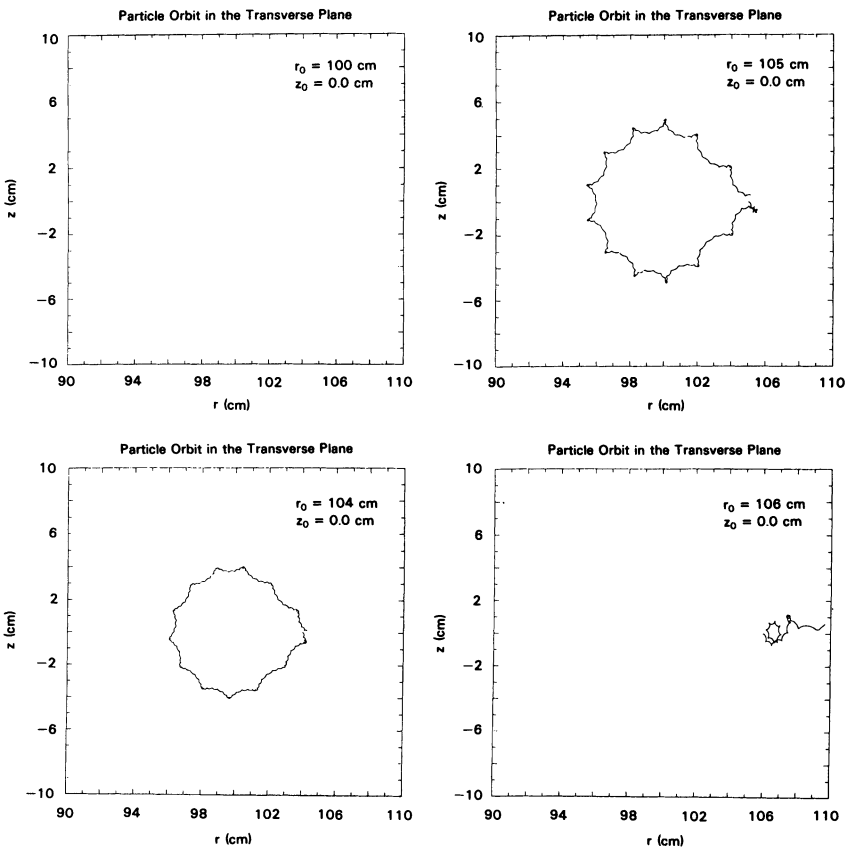

FIGURE 7 Effect of the external field index n_0 of the magnetic field of the plates on the particle orbit, without acceleration. The gap in the outer plate is such that $n_0 \cong 0.5$.

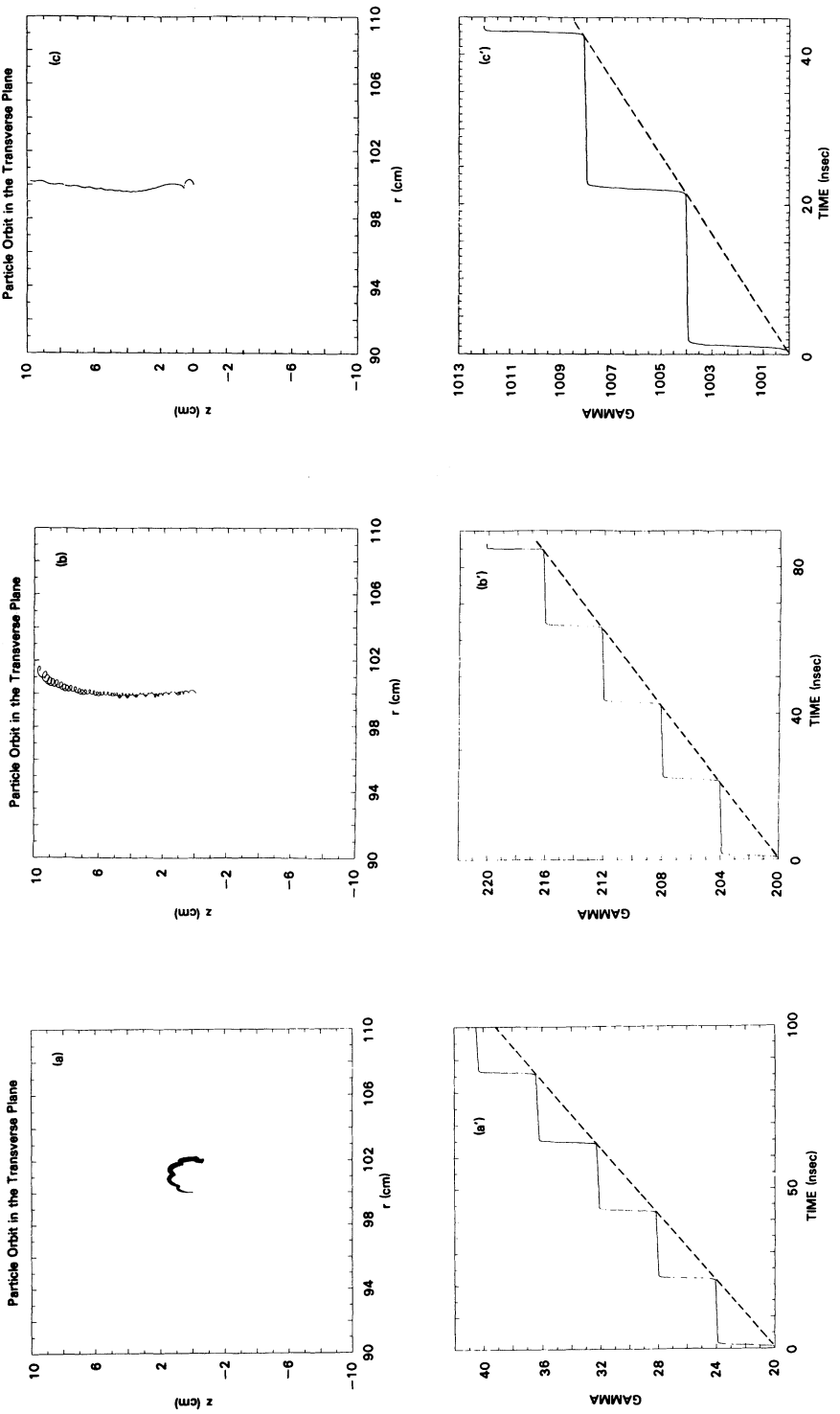

FIGURE 8 Demonstration that the particle orbit is confined by the torsatron fields only at the initial stage of the acceleration. In all cases, there is no gap in the outer plate, so that $n_0 \cong -0.18$.

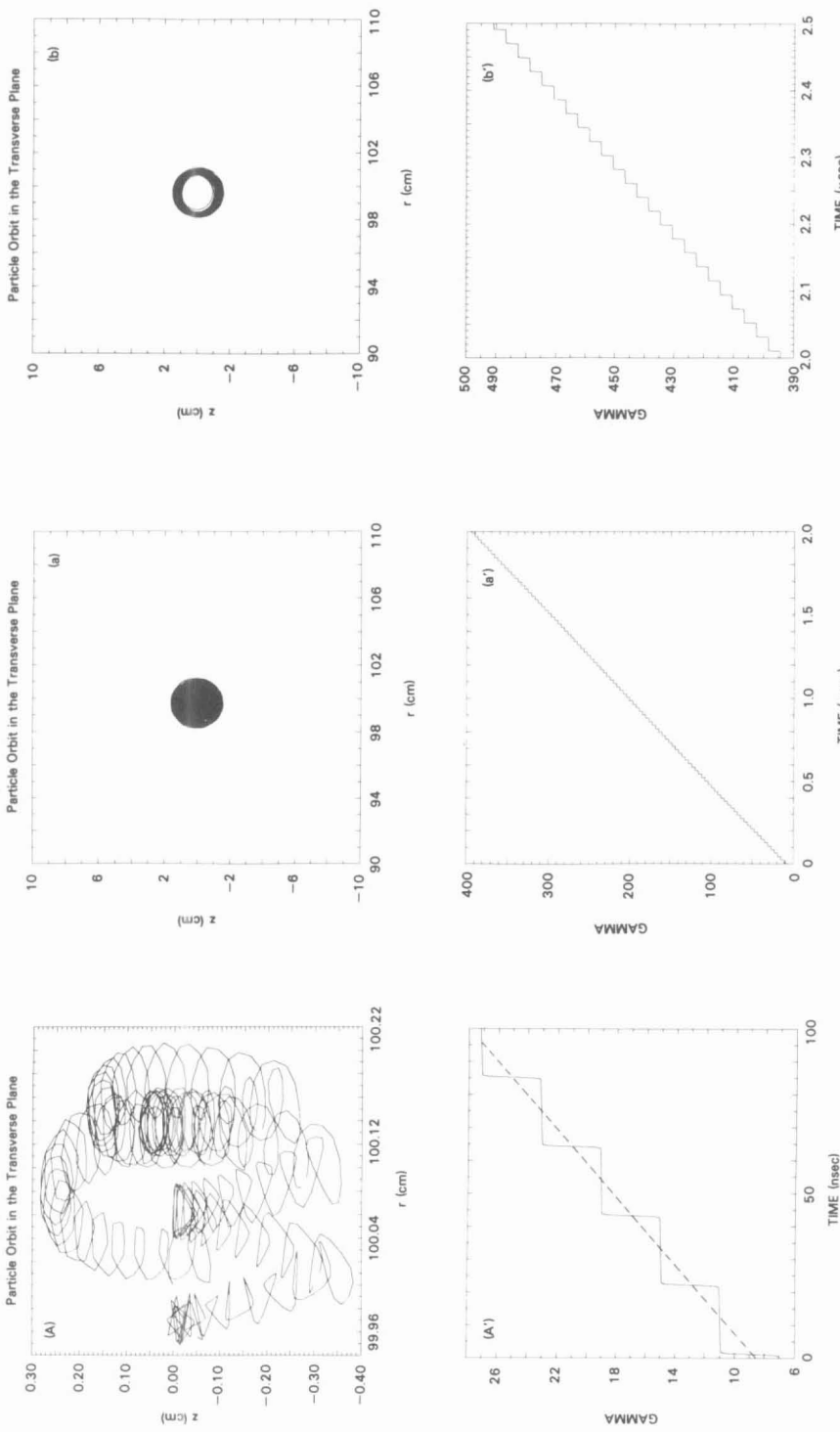

FIGURE 9 Particle orbit on the (r, z) plane (a through f) and the corresponding relativistic factor γ (a′ through f′). The initial position of the particle is at $r = 100$ cm, $z = 0$ cm. The particle orbit and γ at the initial stage of the acceleration are also shown (A and A′).

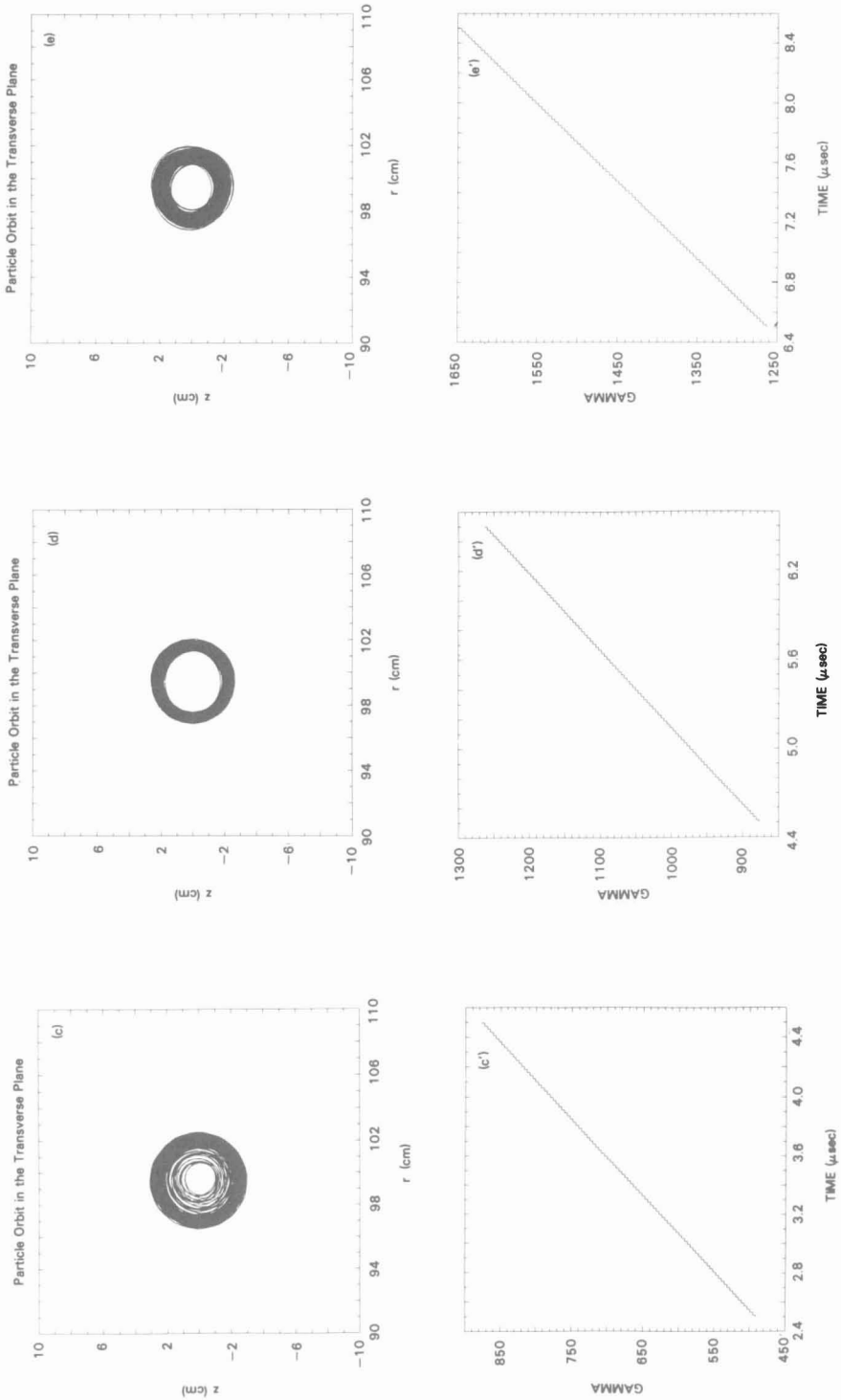

FIGURE 9 *(Continued)*

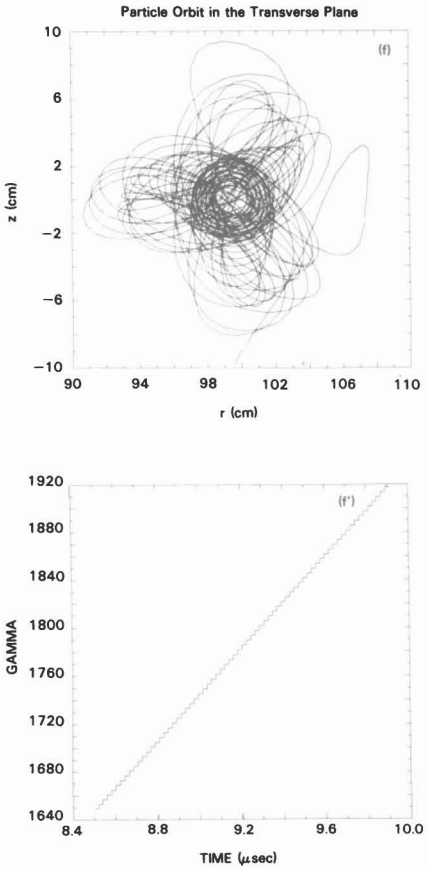

FIGURE 9 (*Continued*)

$\gamma_0 = 200$) in Fig. 8b, and $B_{z0} = 17.05$ kG (it matches $\gamma_0 = 1000$) in Fig. 8c. In all three cases, the rate of change of the current in the plates was equal to $\dot{I}_p = 1.79 \times 10^{11}$ A/s. The linearly increasing vertical magnetic field of the plates matches the dotted lines of γ versus time in Figs. 8a′, 8b′, and 8c′. It is seen then that at low values of γ the torsatron field confines the orbit inside the torus even though the external field index has a negative index. On the other hand, at high values of γ, the torsatron field is no longer effective in confining the particle orbit, which becomes sensitive to the external field index [see Eqs. (30) and (31)].

Figures 9 and 10 provide the main results of this paper. They correspond to two different initial positions of the particle orbit. The various parameters for these computer runs are listed in Table IV. In both cases, the outer plate had a gap so that $n_0 \cong 0.5$ at the minor axis. Figure 9A shows in detail the particle orbit during the initial steps of the acceleration. The dotted line in Fig. 9A′ shows the time-dependent value of γ which matches the linearly increasing vertical magnetic field in the plates. In both runs, a value of γ in excess of 1850 was reached within 10 μs, or within 500 revolutions. In both runs, there was no appreciable drift of

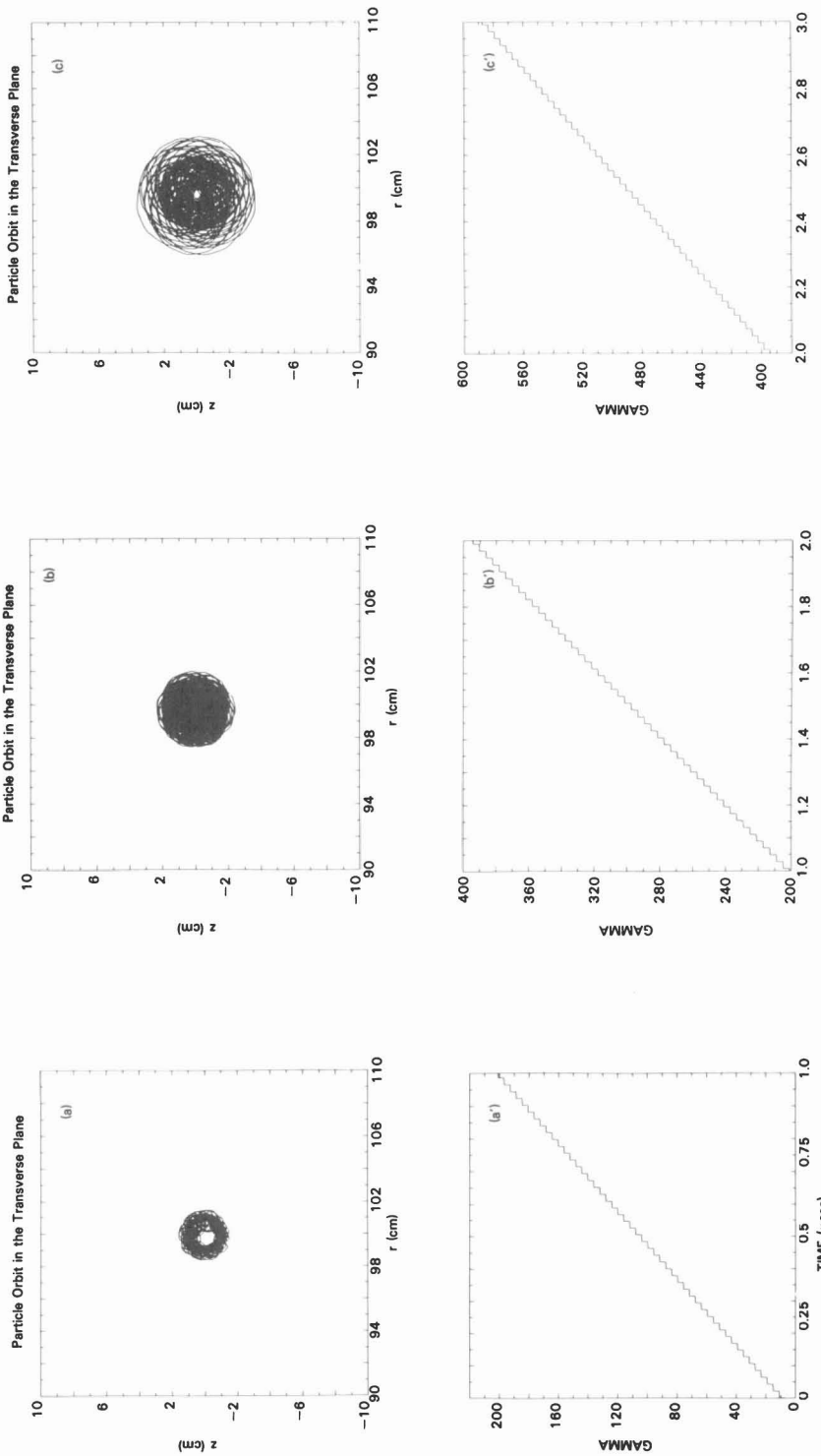

FIGURE 10 Particle orbit on the (r, z) plane (a through j) and the corresponding relativistic factor γ (a′ through j′). The initial position of the particle is at $r = 100$ cm, $z = 1$ cm. The parameters of this run are listed in Table IV.

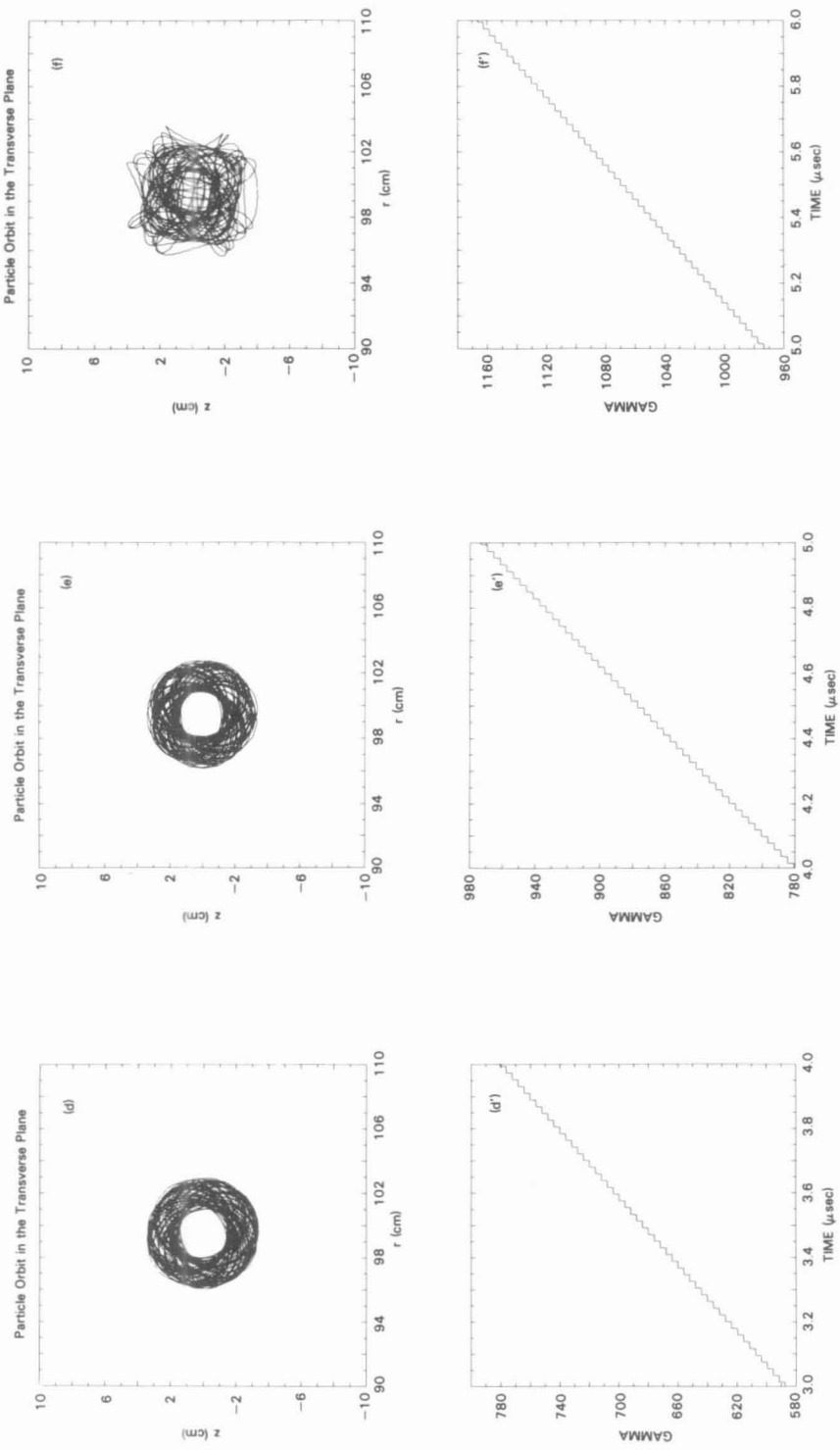

FIGURE 10 (*Continued*)

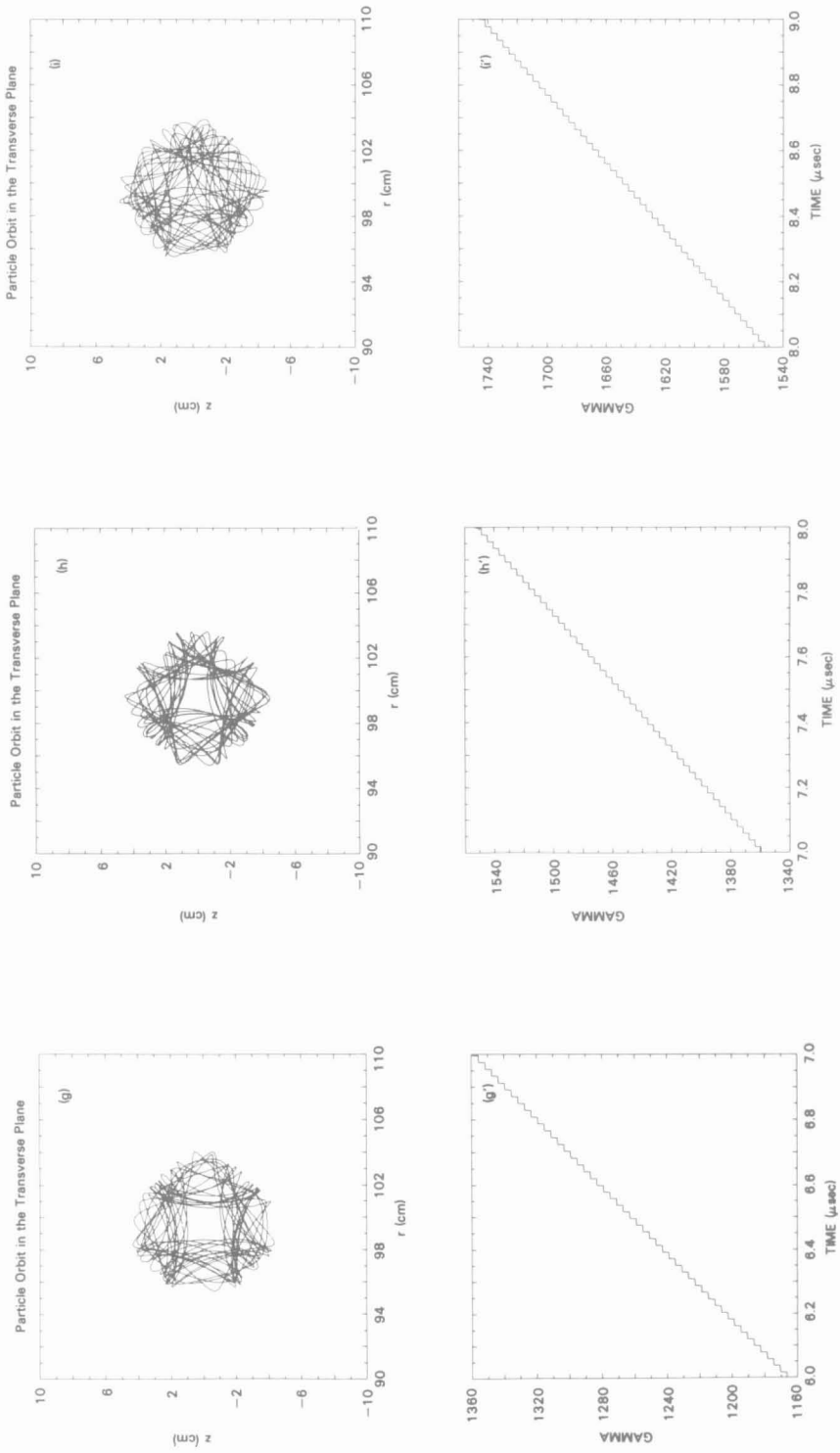

FIGURE 10 (*Continued*)

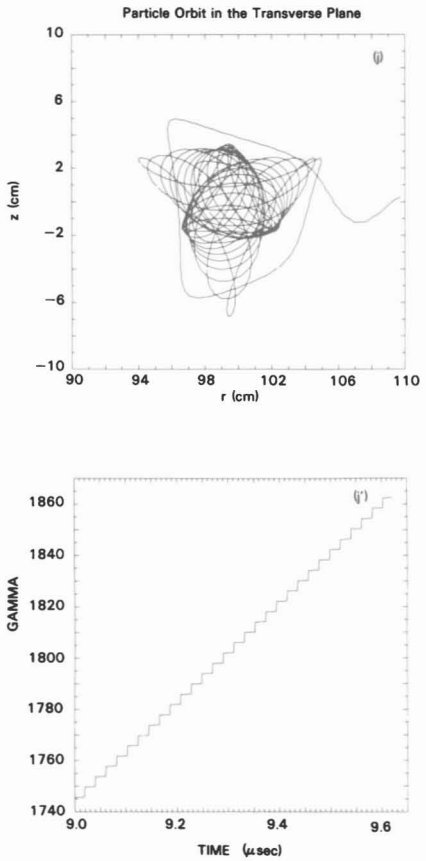

FIGURE 10 (*Continued*)

the particle orbits. As stated in Section 3.2, this is due to the fact that the rate of change of the mismatch $\delta\gamma$ has a second-order dependence on the displacement, and therefore, if $\delta\gamma$ is initially zero, it remains very small during the acceleration. In the initial computer runs, the toroidal corrections of the accelerating field were not included in the computations, and a very slow inward or outward radial drift, as well as an extreme sensitivity to the initial value of the vertical magnetic field and its rate of change, were observed. Values of γ higher than 1000 could not be reached, since the orbits would slowly drift and hit the wall of the torus. After the toroidal corrections were included in the computations, the drift disappeared, as Figs. 9 and 10 indicate.

Another feature that is observed in Figs. 9 and 10 is the expansion of the orbits as time evolves. This is not a continuous expansion but rather it occurs in bursts, the most pronounced being when the value of γ exceeds 1800. As discussed in Section 3.3, in the rebatron there can be resonances [see Eq. [43]] which, for the parameters chosen here, occur at $\gamma_1 = 1830$, $\gamma_2 = 523$, $\gamma_3 = 323$, $\gamma_4 = 236$, etc. The resonance at $\gamma = 1830$, which can be seen clearly in Figs. 9f and 10j,

TABLE IV

Parameters of the Runs Shown in Figs. 9 and 10

Initial current in outer plate, I_p (kA)	8.1
Initial vertical magnetic field from plates, B_{z0} (G)	142.4
Initial matching value of relativistic factor, γ_m	8.35
Rate of change of current in plates, $\dot{I}_p$ (A/s)	1.8745×10^{11}
Accelerating voltage (MV)	−2
Increment of γ per revolution	3.914
Initial relativistic factor, γ	7
Initial positions (cm)	
Fig. 9	$r = 100$ $z = 0$ $s = 0$
Fig. 10	$r = 100$ $z = 1.0$ $s = 0$
Initial velocities	$v_r = 0$ $v_z = 0$ $v_s = -c$

eventually causes the orbit to hit the wall of the torus. This is the worst resonance, and it occurs when $|B_{\theta 0}|/B_{z0} = 1/2$. The amplitude of the nth resonance is proportional to $1/n$ [see Eq. (40)], i.e., it decreases rather slowly with n. Therefore, the higher resonances are also noticeable. The second resonance may be seen in Fig. 9c. Initially, when γ varies from 500 to 600, the orbit rapidly expands from 0.7 cm to 2.2 cm, but as γ keeps increasing from 600 to 900, the radial position of the orbit remains close to 2.5 cm, i.e., it does not vary as much. A comparison of the size of the orbits in Figs. 10b, 10c, and 10d indicates that there is a resonance close to $\gamma = 500$ in the second run, too. Resonances beyond the second are clustered much closer together, their amplitudes are smaller, and therefore they are not as noticeable individually. But they do cause an expansion of the particle orbit, as indicated in Fig. 9a and in Figs. 10a and 10b. The value of the total toroidal magnetic field used in these runs was $B_{\theta 0} = -15.6$ kG. A higher value of $B_{\theta 0}$ would cause the first resonance to occur at a value of γ greater than 1830 [see Eq. (43)]. Therefore, there is no intrinsic difficulty in the rebatron in accelerating the beam to 1 GeV and beyond.

Figure 9f indicates a radical change in the shape of the particle orbit as the value of γ exceeds 1800. A similar observation holds for Fig. 10j and for Fig. 10f, where γ is in the neighborhood of 1100. As stated in Section 3.3, this is due to the fact that the characterisitc frequencies become multiples of each other. For the

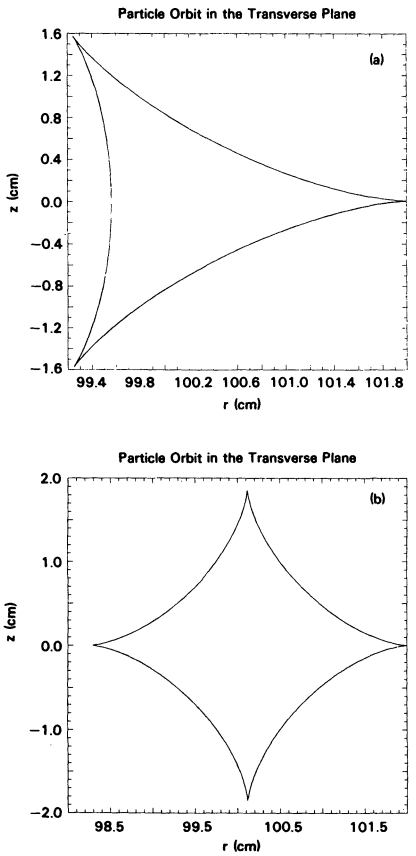

FIGURE 11 Particle orbits without acceleration, when the characteristic frequencies of the system become a multiple of each other. This occurs at $\gamma_2 = 1830$(a) and $\gamma_3 = 1121$(b).

parameters chosen here, Eq. (45) predicts that multiple frequencies should occur when $\gamma_2 = 1830$, $\gamma_3 = 1121$, etc. Notice that in the first run there is no change at $\gamma = 1121$. This indicates that, in addition to the occurrence of a multiple frequency, some other conditions must be satisfied in order to change the shape of the orbit. A clear demonstration of the multiple frequency effect is given in the runs shown in Figs. 11a and 11b, where there is no acceleration. In both runs, the initial position is $x_0 = 2$ cm, $z_0 = 0$, and the initial velocity is $v_x = v_z = 0$, $v_\theta = c$. Also, in both runs, $n_0 = 1/2$. In the run of Fig. 11a, $\gamma = 1830$ and $B_{z0} = 31.167$ kG (it matches $\gamma = 1830$), while in the run of Fig. 11b, $\gamma = 1121$ and $B_{z0} = 19.095$ kG (it matches $\gamma_0 = 1121$).

5. CONCLUSIONS

A detailed numerical and analytical investigation of the beam dynamics in the rebatron accelerator has been carried out. It has been shown that energies

approaching 1 GeV can be achieved within 10 μs . Since the acceleration occurs in such a short time, the device may not be sensitive to the various inabilities, and the loss to synchrotron radiation should be small.

As a result of the periodic nature of the acceleration in the rebatron, it has been found that resonances can be excited which cause the orbits to expand, and, in the worst case, the beam may hit the wall of the toroidal chamber. The worst resonance is the fundamental, i.e., $n = 1$, and it occurs when the vertical magnetic field becomes twice the total toroidal magnetic field. This could be a potential problem in the rebatron unless the toroidal magnetic field is sufficiently high that the fundamental resonance is not excited. In the cases studied here, the total toroidal magnetic field was set at 15.6 kG, which allowed the beam to be accelerated to a γ slightly higher than 1800 before the fundamental resonance was reached at $\gamma_1 = 1830$. From the computer runs, it has been concluded that the higher resonances cause the orbits to expand but that they are not as detrimental as the fundamental resonance.

To keep the inductive voltage manageable, the vertical plates which generate the vertical magnetic field should have a low inductance. As an example, for the parameters in Table II, the inductance L_p of the plates is approximately[28] 2.5 μH. A vertical magnetic field $B_{z0} = 17$ kG is required to reach a γ of 1000, while the plates generate 17.58 G per kA at the minor axis. Therefore, the current in each plate required to generate 17 kG is $I_p = 967$ kA. Suppose that the acceleration time $\Delta t = 10\,\mu$s. Then the rate of change of the current in the plates is $\dot{I}_p = 0.967 \times 10^{11}$ A/s, and the inductive voltage is $V_p = 242$ kV, which is fairly high.

The simple analytical model of Section 3 has provided quite reliable results with regard to the confinement of the beam by the torsatron magnetic field. The predictions of the model are in good agreement with the numerical results. It has been shown that, at the initial stage of the acceleration, the torsatron field provides excellent confinement of the beam, and the beam equilibrium position was quite insensitive to the mismatch $\delta\gamma/\gamma$ and to the external field index n_0, as long as $\omega_w \ll |\Omega_{\theta 0}/\gamma|$. As the beam energy increases, the stage is reached where $\omega_w \gg |\Omega_{\theta 0}/\gamma|$. The torsatron field is no longer effective, and the beam equilibrium position becomes sensitive to both the mismatch $\delta\gamma/\gamma$ and the external field index n_0. As mentioned in Section 3.2, the sensitivity to n_0 may prove beneficial in providing a means for extracting the beam. (see Figs. 8b and 8c).

Another interesting feature of the acceleration in the rebatron is the absence of any drift of the beam when the vertical magnetic field is matched to the beam energy. As explained in Section 3.2, this is due to the fact that the first-order toroidal correction of the accelerating field cancels the first-order correction of the electric field from the plates. Therefore, if the mismatch is initially zero, it will remain very small during the acceleration, and there is no drift. This has been verified in several computer runs.

In the analytical and numerical results presented in this paper, the image fields of the beam have not been included. Their effect on the beam dynamics and the acceleration process will be the subject of a future publication.

REFERENCES

1. C. A. Kapetanakos and P. Sprangle, *Phys. Today* **38** (2), 58 (Feb. 1985).
2. C. A. Kapetanakos and P. Sprangle, NRL memo report No. 5259 (1984).
3. J. E. Leiss, *IEEE Trans. Nucl. Sci.* **NS-26,** 3870 (1979).
4. J. A. Nation, *Particle Accelerators* **10,** 1 (1979).
5. D. Keefe, *Particle Accelerators* **11,** 197 (1981).
6. N. C. Christofilos et al., *Rev. Sci. Instrum.* **35,** 886 (1964).
7. J. E. Leiss, N. J. Norris, and M. A. Wilson, *Particle Accelerators* **10,** 223 (1980).
8. T. J. Fessenden et al., *Proc. Intern. Topical Conf. on High Power Electron and Ion Beam Research and Technology,* Palaiseau, France, June 29–July 3, 1981, p. 813.
9. R. J. Briggs et al., *IEEE Trans. Nucl. Sci.* **NS-28,** 3360 (June 1981).
10. A. I. Pavlovskii et al., *Sov. Phys. Dokl.* **25,** 120 (1980).
11. K. R. Prestwich et al., *IEEE Trans. Nucl. Sci.* **NS-30,** 3355 (1983).
12. L. N. Kazanskii, A. V. Kisletsov, and A. N. Lebedev, *At. Energ.* **30,** 27 (1971).
13. M. Friedman, *Appl. Phys. Lett.* **41,** 419 (1982).
14. D. W. Kerst, *Nature* **157,** 90 (1946).
15. A. I. Pavlovskii et al., *Sov. Phys. Tech. Phys.* **22,** 218 (1977).
16. P. Sprangle and C. A. Kapetanakos, *J. Appl. Phys.* **49,** 1 (1978).
17. N. Rostoker, *Comments Plasma Phys.* **6,** 91 (1980).
18. C. A. Kapetanakos, P. Sprangle, D. P. Chernin, S. J. Marsh, and I. Haber, *Phys. Fluids* **26,** 1634 (1983).
19. C. W. Roberson, A. Mondelli, and D. Chernin, *Phys. Rev. Lett.* **50,** 507 (1983).
20. A. A. Mondelli and C. W. Roberson, *Particle Accelerators* **15,** 221 (1984).
21. C. A. Kapetanakos et al., NRL memo report No. 5503 (1985); also *Particle Accelerators* **18,** 73 (1985).
22. M. G. Mazarakis et al., *IEEE Trans. Nucl. Sci.* **NS-32,** 3237 (1985).
23. L. Teng, Argonne National Laboratory report No. AnLAB-55 (1959); G. Salardi et al., *Nucl. Instrum. Methods* **59,** 152 (1968); R. M. Pearce, *Nucl. Instrum. Methods* **83,** 101 (1970); R. L. Gluckstern, Proc. Linear Accelerator Conf., 1979, p. 245.
24. P. Sprangle and C. A. Kapetanakos, NRL memo report No. 5458 (1984).
25. C. A. Kapetanakos, D. Dialetis, and S. J. Marsh, NRL memo report No. 5619 (1985).
26. I. S. Gradshteyn and I. M. Ryzhik, *Table of Integrals, Series, and Products* (Academic Press, New York, 1980) pp. 905–906, Eqs. 8.113 and 8.114.
27. D. Chernin and P. Sprangle, *Particle Accelerators* **12,** 101 (1982).
28. H. Knoepfel, *Pulsed High Magnetic Fields* (North-Holland, Amsterdam, 1970), p. 323, Fig. A1.21.